The use of fine water sprays to suppress fume emissions when casting ferromanganese

Sarel J. Gates*[1], Gerrit Kornelius[1], Steven C. Rencken[1], Neil M. Fagan[1], Peter Cowx[2], Luther Els[3]
[1]University of Pretoria, Dept of Chemical Engineering,Environmental Engineering Group,
Private Bag X20 Hatfield, Pretoria, South Africa, 0028, gerrit.kornelius@up.ac.za
[2]Eramet Norway, Sauda, Norway, peter.cowx@erametgroup.com
[3]Resonant Environmental Technologies, P.O. Box 12225, Centurion, South Africa, 0046, luther@resonant.co.za

Received: 14 October 2015 - **Reviewed:** 26 November 2015 - **Accepted:** 30 November 2015
http://dx.doi.org/10.17159/2410-972X/2015/v25n2a3

Abstract
During the casting of ferromanganese alloys from electric arc furnaces into sand beds at temperatures of up to 1800°C a considerable amount of very brown fumes are generated when the alloy fume is oxidized in the atmosphere. The fume is difficult to capture because of the large flux of gas that is generated. Possible reasons for this flux include the high evaporation rate of Mn at elevated temperatures, the large surface area of the casting beds and the large thermal plumes over the furnace tapholes and casting beds. It has been found that the use of fine water sprays along the edge of the roof that covers the casting bed resulted in a significant reduction in visible emissions. This paper describes research into the kinetics of the fume to improve the design of the capture hoods, as well as the mechanism of suppression by the water sprays by using CFD analysis. It is shown that the oxidation reaction produces less than 20% of the energy content of the plume over the arc furnace taphole, and also that radiation heat transfer may play an important role in increasing the energy content of the taphole plume. The capture of fume particles by fine spray droplets is shown to have limited efficiency, while the heat sink that is caused by evaporation does not materially contribute to the circulation of fume through the spray. It is postulated that the increased moisture content of the air over the casting beds may be instrumental in reducing the oxygen partial pressure or in the formation of an oxide layer, both of which would reduce metal evaporation and, therefore fume formation. The exact mechanism requires further investigation.

Keywords
ferromanganese, secondary fume, water sprays, fume capture hoods, fume extraction, ferro-alloy tapping

Introduction
Eramet Sauda, in Norway, operates two ferromanganese furnaces producing high carbon ferromanganese (HCFeMn) as well as a Manganese Oxygen Refining (MOR) unit to produce medium and low-carbon ferromanganese (LCFeMn). Secondary fume emissions occur at the tapholes of the arc furnaces as well as during post-taphole operations. The current secondary fume capturing system has good capacity, but emissions do still escape from the furnace building. Due to their small particle size, manganese oxides that are present in these fumes pass through the trachea and bronchi to the lungs (de Nevers 2010). Health risks include manganism, a serious and irreversible brain disease, and various lung disorders. It is therefore important to either suppress or capture the fumes formed during casting operations (Goodfellow et al. 2001). The formation mechanism of the fumes was investigated in order to understand its possible contribution to the fume emission volume and energy content. A study was then conducted to investigate whether a fine water spray can suppress fume emissions from casting bed operations and, consequently, mitigate Mn_3O_4 pollution without enclosing the sand beds or significantly increasing the fume capture capacity. To achieve this, flat jet sprayers were placed on the edge of the shed roof that cover the casting beds. These sprayers sprayed horizontally away from the shed to form a water curtain on the outside of the shed without water accumulation in the shed.

Theoretical Background

Fume Energy Contributions

Mechanisms and Fume Formation
Little information on the fume generation mechanisms in the ferromanganese industry could be found, but studies in other similar applications suggest that the predominant mechanisms in steelmaking are bubble bursting and volatilisation (Guézennec et al. 2004; Huber et al. 2000; Gonser et al. 2011). There is little bubble formation during the metal flow, from one casting pocket to the next. Due to the high metal temperatures and the low relative boiling point of Mn, evaporation and oxidation to Mn_3O_4 is considered the most significant mechanism of the fume generation. Mn_3O_4 has the highest Gibbs Free energy of the manganese oxides, making it the most likely product to form at

the elevated temperatures found during casting operations (Els et al. 2013).

The energy generated by the reaction involved in the Mn_3O_4 formation, can be assumed to contribute to the fume's energy. A discussion of the reaction kinetics involved in the Mn_3O_4 formation will help in the understanding of the unexpected high energy content of the fumes, the fumes' rise velocity and the necessary extraction required to ensure that the fumes are captured.

Lee et al. (2005) considered various reaction-limiting factors for the fume formation in the casting of the high carbon FeMn produced in the arc furnace. They found that the Mn in the melt is essentially lost through evaporation and oxidation to form MnO mist, which is further oxidised to Mn_3O_4 particulate. Turkdogan et al. (1963) studied the diffusion-limited rates of vaporization of metals and showed that at high oxygen partial pressures, metal evaporation rates approach those in a vacuum and can be predicted by the Langmuir equation:

$$E_a = p_a \left(\frac{M_a}{2\pi RT}\right)^{0.5} \quad (1)$$

where R is the gas constant, T the absolute temperature, E_a and M_a the evaporation rate and the molar mass of a respectively (Turkdogan et al. 1963; Dennis et al. 2001)[1]. This effect is known as oxidation enhanced vaporization and is caused by the oxidation of the metal vapour above the liquid surface (Turkdogan et al. 1963) to form the MnO mist, reducing the Mn concentration in the gas-liquid interface and promoting further evaporation of Mn into this sink.

In reality the O_2 concentrations may not be high enough to cause O_2 enhanced oxidation. Lee et al. (2005) suggest that no MnO mist and, therefore, no Mn_3O_4 forms when the O_2 partial pressure is below 17kPa, which may be the case where decarburisation of HCFeMn occurs during tapping.

The possible rate limiting factors are the mass transfer of Mn in the melt to the gas-liquid interface, evaporation of Mn at the interface, Mn vapour transport away from the interface and transport of O_2 to the interface. The high metal temperature ensures that the evaporation of Mn is fast. Because of the relative abundance of Mn in the melt, it is not likely to be depleted at the metal surface. Therefore the MnO fume formation rate is considered to be controlled by the counter-diffusion of Mn and O_2 in the boundary layer above the metal surface (Dushman et al. 1962), which can be expressed mathematically with:

$$J_{Mn} = J_{O_2} = \frac{h_{Mn}}{RT}\left(P_{Mn}^{sat} - p_{Mn}\right) \quad (2)$$

where J_{Mn} is the evaporation flux of the Mn, J_{O_2} the flux of O_2 to the gas-liquid interface, $h_{Mn} = D_{Mn}/l$ the average mass transfer coefficient of the Mn vapour and p_{Mn} the partial pressure of Mn at the top of the mass transfer boundary layer (l).

[1] Unless indicated otherwise, all equations are expressed in SI units

According to Lee et al. (2005), the affinity of O_2 with Fe (at high temperatures) is approximately two orders of magnitude less than that of Mn, rendering the formation of FeO negligible.

Radiation Effects

The net rate of radiation can be expressed with the following equation (Çengel et al. 2011; Welty et al. 2009):

$$Q = \sigma\varepsilon A_s T_s^4 - \sigma\alpha A_s T_{surr}^4 \quad (3)$$

where σ is the Stefan-Boltzmann constant ($5.67\times10^{-8}\ W/(m^2 \cdot K^4)$), ε the emissivity of the surface, A_s the surface area, α the absorptivity of the surface, T_s and T_{surr} the temperatures of the surface and surroundings, respectively.

Due to the significant difference between the temperature of the melt and its surroundings, the amount of energy released from the melt in the form of thermal radiation is high. The energy transfer rate varies between 100kW/m^2 and 300kW/m^2, depending on the metal's surface temperature and the emissivity. It is improbable that the melt will absorb a significant amount of energy (Els et al. 2013).

The generated fumes primarily consists of Mn_3O_4 particulates, which results in the hazy appearance. Non-polar gasses are virtually unaffected by radiation effects, whilst polar molecules are capable of absorbing radiation (Çengel et al. 2011; Modest 2003). With the above-mentioned in mind, the thermal radiation will be dependent on the Mn_3O_4 particulate content of the fumes. Energy may be reflected by the particulates and may further be re emitted. The exact effects of the particulate presence in the plume are at this stage difficult to quantify.

Natural Convectional Effects

As Els et al. (2010) describe, the majority of fume extraction systems are designed based on flow rates calculated from thermal updrafts which are caused by convection. The convective heat transfer rate is calculated by using *Equation* (4) (Çengel et al. 2011):

$$\Phi = hA_s(T_s - T_\infty) \quad (4)$$

where h is the convective heat transfer coefficient, A_s the surface area of the melt, T_s and T_∞ the surface temperature and surrounding air temperature respectively (Çengel et al. 2011).

Furthermore, there is also natural convective heat transfer between the air and the droplets from the water spray, where a spraying system is used.

Water Spray System

Overview

To attempt to reduce the amount of fugitive secondary fumes formed during casting of ferromanganese on casting beds, Els et al. (2014) studied the possibility of implementing air curtains, enlarging the extraction volume or extending the tapping

shed structure. As expected, the efficiency increases when the operational area is enclosed or the extraction volume is increased. Some of the experimental runs that use air curtains also show promising results. In an attempt to find a more efficient alternative, water sprays were installed at the casting beds at Eramet Sauda. The implementation of a water curtain was found to visibly reduce the fume concentration over the casting beds. Two mechanisms were thought to influence the secondary fume.

The first involves the suppression of fume emissions because of the water spray acting as a heat sink, which enhance convectional effects. The air density in the vicinity of the water droplets tends to increase as the air temperature decreases, resulting in buoyancy effects playing a role. The change in circulatory pattern and/or the increased humidity of the air is believed to be involved in the enhanced rate of formation of an oxide layer on the molten metal, thereby reducing the rate by which fumes form. This will be discussed further under *Heat Transfer Effects* on this page.

The second postulated effect of the water spray may comprise the mass transfer of Mn_3O_4 particles from the fumes to the water droplets. It is expected that the Mn_3O_4 particulates will be captured by the water droplets, and then settle on the floor. Thereafter appropriate processing actions may be taken to manage the Mn_3O_4 particles.

Computer Fluid Dynamics (CFD) Modelling

Due to the complex flow patterns of the fumes, a computational model is necessary to efficiently determine the air flow patterns (Witt et al. 2006). CFD modelling was therefore used to simulate the fumes rising off the casting beds and the effect of the water spray. The simulations were performed using FloEFD 14.1.0 (Mentor Graphics 2015). Figure 1 provides a CFD simulation of the temperature profile over a casting bed, where the water spray system (situated at the edge of the roof over the casting bed) is inactive. The CFD simulation delivered comparable results to the on-site measurements of the fugitive fumes' temperature. The air flow patterns of this base case were compared to the air flow patterns when the spray system was activated and the spray acted as a heat sink.

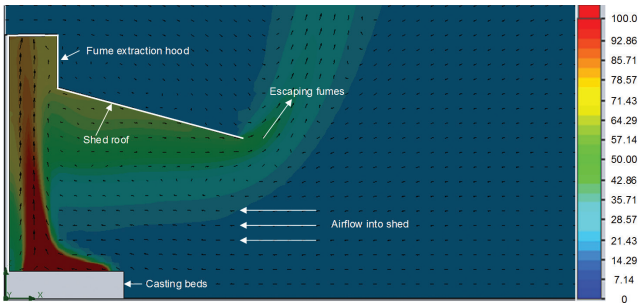

***Figure 1**: Base case CFD showing the temperature with the scale on the left.*

Spray Pattern Development

The amount of heat and mass transfer effects of the spray depends on the spray area. Spray area determination requires modelling of the droplet trajectory. Droplets were assumed to be homogenous in size and shape after dispersion from the spray. It is reasonable to assume that heat transfer effects will have the largest effect at the top of the shed where the highest temperature occurs. The initial horizontal velocity of the droplet can be determined by *Equation* (5):

$$v_d = \frac{Q_d}{A} \quad (5)$$

where v_d is the velocity Q_d the water volumetric flowrate and A the open area of the spray nozzle. Once dispersed, the horizontal velocity of the droplets decreases exponentially due to drag force effects. Two possible relationships between C_d and the Re_d are expressed in *Equations* (6) and (7) (de Nevers 2010):

$$C_d = \frac{24}{Re_d}, Re_d < 0.3 \quad (6)$$

$$C_d = \frac{24}{Re_d}(1 + 0.14R_d^{0.7}), 0.3 \leq Re_d \leq 1000 \quad (7)$$

where Re_d is the dimensionless Reynolds number which can be calculated with (Çengel et al. 2011):

$$Re_d = \frac{\rho D_d v_d}{\mu} \quad (8)$$

where ρ is the fluid density, D_d the droplet diameter and μ the fluid viscosity.

Since the decrease in the droplets' velocity is much greater than its decrease in the diameter, it is assumed that the droplet's diameter remains constant when the area of water dispersion is calculated. The horizontal velocity of the droplets was modelled in time increments of 0.1s until the horizontal component of the velocity has decreased to zero. This implies that only vertical forces are still active after this point.

For reasons of simplicity, it is assumed that the time it takes until the droplet is influenced only by vertical forces is negligible in comparison with the total falling time. For the transfer of particulate to the droplets, a homogenous dispersion of droplets is assumed to fall vertically from the roof height to the floor over the entire spray area. Finally, the spray area is calculated as the product of the shed roof length and the horizontal distance that the droplets travel.

Heat Transfer Effects

Balances:

By assuming that the heat which is transferred to the water is the same as the heat that is lost through hot air escaping from underneath the shed roof in a steady state operation, and that the kinetic and potential energies are negligible, the energy balance reduces to *Equation* (9):

$$\sum M_{in} C_{p_{in}} T_{in} = \sum M_{out} C_{p_{out}} T_{out} \quad (9)$$

where C_p is the specific heat capacity at constant pressure, M the mass, and T the absolute temperature.

Noting that the particulate concentration is low, the mass balance becomes:

$$M_{a_{in}} + M_{\mathcal{H}_{in}} + M_{w_{in}} = M_{a_{out}} + M_{\mathcal{H}_{out}} + M_{w_{in}} \quad (10)$$

where M_a, M_H and M_w represents the mass of dry air, water vapour in the air and water from the sprayers respectively.

Humidity

Absolute humidity is defined as the mass of water vapour per unit of dry air and can be expressed mathematically for an air-water system as in *Equation* (11) (Green et al. 2007):

$$\mathcal{H} = \frac{0.622 p_v}{P - p_v} \quad (11)$$

where p_v is the vapour pressure of water at a given temperature and P the total pressure of the air-water system. The evaporation rate of the water droplets is dependent on the humidity of the air.

Drop Diameter

It is further assumed that the water and air are at thermal equilibrium as it leaves the control volume. Therefore, the temperature of the water and air will be equal. According to Holterman (2003), a droplet's temperature will decrease as it falls through the air as a result of evaporation and will continue to decrease until the water reaches the wet-bulb temperature. The difference in temperature of the droplets and the air results in energy transfer, with the droplets acting as heat sinks. This transfer of heat may affect the droplet's diameter significantly. Various models describing the change in droplet diameter have been developed by Ranz et al. (1952), Goering et al. (1972) and by Williamson et al. (1974). Williamson (*ibid.*) proposed using *Equation* (12) to determine the change in droplet diameter:

$$\frac{dD_d}{dt} = -\frac{4MW_L D_{v,f}}{D_d \rho_d R T_f} \Delta p \left(1 + 0.276 R e_d^{\frac{1}{2}} Sc^{\frac{1}{3}}\right) \quad (12)$$

where MW_L is the molecular weight of the evaporating liquid, ρ_L the density of the drop, $D_{v,f}$ the average diffusion coefficient for the vapour molecules in the saturated film around the drop, T_f the average absolute temperature in the film, Re the Reynolds number, Sc the Schmidt's number, Δp the difference between the vapour pressure near the drop and at the ambient atmosphere and R the gas constant.

It is assumed that the heat transfer effects will result in the droplets to evaporate uniformly. Diffusivity dependence on temperature is given by *Equation* (13) (Welty et al. 2009):

$$D_{AB} \propto T^{\frac{3}{2}} \quad (13)$$

Schmidt's number is defined as (Çengel et al. 2011):

$$Sc = \frac{\mu_{a,f}}{\rho_{a,f} D_{v,f}} \quad (14)$$

where the subscript f indicates that the given properties is at the film temperature.

Mass Transfer Effects

Mass transfer occurs when Mn_3O_4 particulates come into contact with the water droplets. The droplet size as well as the particle characteristics influence the capture efficiency. Furthermore, the water curtain is dependent on the nozzle type (Grant et al. 2000; Nuyttens et al. 2007). Flat jet K 1590 type nozzles are installed at Eramet Sauda. The control volume for the material balance is illustrated in Figure 2, adapted from de Nevers (2010)

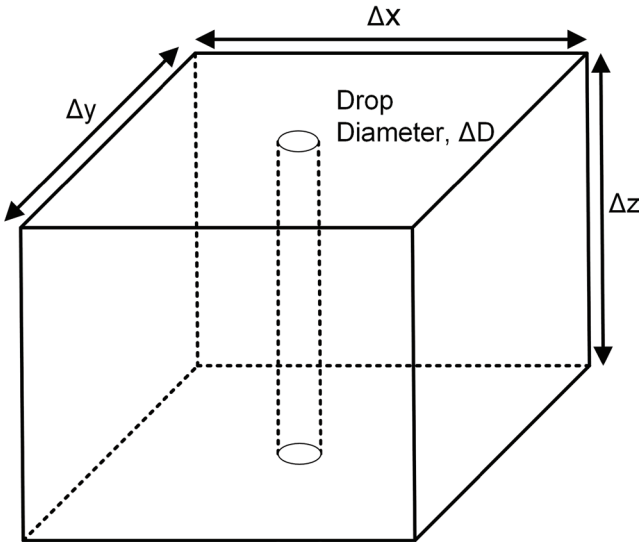

***Figure 2**: Control volume (de Nevers 2010)*

Particulate Distribution

A chemical analysis of the fumes showed that Mn_3O_4 formed about 97% of the total mass. The particle size distribution (PSD), shown in Figure 3, was measured by laser diffraction. The particles have a mean diameter of about 0.6µm.

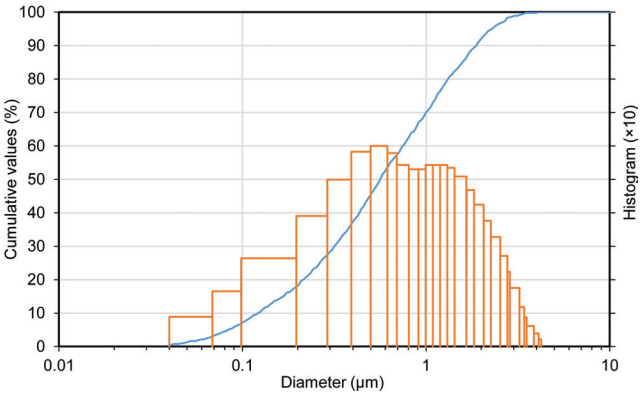

***Figure 3**: Particle size distribution for the fume*

Water Droplet Characteristics

It is assumed that for each Δz increment, the droplet characteristics remain constant in terms of diameter and droplet shape. Further assuming that the droplet is spherical, the volume through which the droplet falls can be calculated by

(de Nevers 2010):

$$V_{swept} = \frac{\pi}{4} D_d^2 \Delta z \quad (15)$$

where V_{swept} is the sweeping volume, D_d the droplet diameter and Δz the incremental length.

Assuming spherical droplets and uniform distribution of the fume particulate in the air, the efficiency of particle capture, as illustrated graphically in Figure 4 (Kopita 1955).

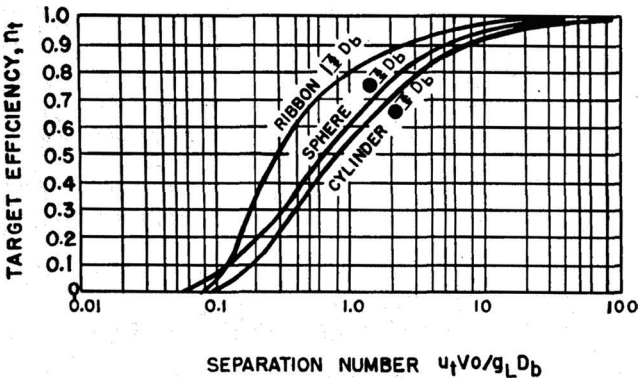

***Figure 4**: Target efficiency correlation (Kopita 1955)*

The separation number can be calculated with *Equation* (16) adapted from de Nevers (2010):

$$N_s = \frac{\rho_p D_p^2 v_{d,t}}{18 \mu_g D_d} \quad (16)$$

where D_p is the diameter of the particle, μ_g the viscosity of the plume and $v_{d,t}$ the terminal velocity of the droplets. Once the target efficiency is known, the mass of particles absorbed can be calculated with *Equation* (17) (de Nevers 2010):

$$M_{transfered} = \frac{\pi}{4} D_d^2 \Delta z c \eta_t \quad (17)$$

where c represent the particle concentration which can be calculated with *Equation* (18) (de Nevers 2010):

$$\frac{dc}{dt} = -\frac{1.5 c \eta_t Q_d}{D_d A} \quad (18)$$

where η_t is the target efficiency, Q_d the volumetric flowrate of the water droplets, D_d the droplet diameter and A the spray area.

The initial particle concentration is estimated as the concentration that is measured when the sprayer system is inactive. If the initial concentration is known, the above equation can be solved without difficulty. The remaining concentration is a function of time, which is determined by the water droplet's settling velocity. Because the droplets are small, they will rapidly reach their terminal settling velocity; the assumption is therefore made that the droplets reach terminal settling velocity at the edge of the shed roof.

Acting Forces on the Water Droplet

Considering the forces acting on the water droplets, Newton's second law of motion reduces to *Equation* (19) (de Nevers 2010).

$$ma = \rho_d \left(\frac{\pi}{6}\right) D_d^3 g - \rho_{fluid} \left(\frac{\pi}{6}\right) D_d^3 g - F_d \quad (19)$$

where m is the mass of a water droplet, a its acceleration, ρ_d its density, g the gravitational constant, ρ_{fluid} the density of the fluid (in this case air) through which the droplets falls and F_d the drag force. According to Çengel et al. (2011), the general equation for the relationship between the drag coefficient (C_D) and the drag force (F_d) is given by:

$$F_d = \frac{1}{2} C_D \rho_{fluid} v_d^2 A \quad (20)$$

where A represents the spray area, ρ_{fluid} the fluid density and v_d the droplet velocity. Together with the relationship between the Reynolds number and the drag coefficient for spherical droplets, this can be used to calculate the terminal velocity for each of the assumed droplet sizes. The effectiveness of the spray system can then be found from:

$$\eta_{overall} = \frac{c_0 - c}{c_0} \times 100 \quad (21)$$

Summary

To be able to design a more efficient extraction system, it is necessary to know the extent of fume formation and how energy contributors (heat of formation, radiation and natural convection) will effect these fumes. The Mn formation is suspected to be controlled by the diffusion of the Mn through the gas-liquid interface, although Lee et al. (2005) indicates that no Mn vapour will form if the oxygen partial pressure is below 17kPa.

Various attempts to reduce the secondary fumes have led to the conclusion that the fumes will be captured by increasing the extraction volume or designing a closed structure in which casting operations will occur. These solutions are however expensive. In an attempt to find a more efficient and cost effective solution, Eramet Sauda installed water sprayers. As a result fume emissions were visibly reduced.

Two possible mechanisms were investigated which may be influential in the water curtain's ability to visibly reduce secondary fumes over the casting beds. The first involved the heat transfer between the fumes and the water spray, which were affected by the energy content of the fumes, the humidity of the air and the change in the droplet's diameter. The second possible mechanism was the mass transfer of Mn_3O_4 particulates from the fume to the droplets, which were affected by the particle's and droplet's characteristics as well as the forces acting on the droplet. CFD simulations were used to model the effects of the reduction mechanisms on the air flow patterns and compare the obtained results with the base case where the water spray system was not used.

Results and Discussion

Plant Specific Information

The parameters shown in Table 1 are the characteristics of the spray system and environment.

***Table 1**: Parameters at Eramet Sauda*

Description	Value	Units
Total pressure	101.3	kPa
Hot air temperature	45	$°C$
Ambient temperature of the air	20	$°C$
Water temperature	12	$°C$
Relative humidity at ambient air temperature	70	%
Droplet diameter	250	μm
Height of shed roof	6	m
Sprayer spacing along the roof	2	m
Water flowrate out of the sprayers	15	L/min

Figure 5 provides a schematic representation of the shed and sprayer system.

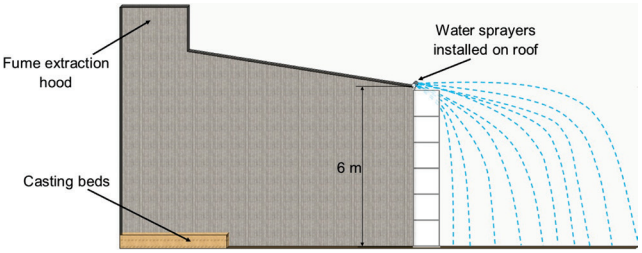

***Figure 5**: Schematic of shed and sprayers*

Note the 1m by 1m control volume blocks extending vertically beneath the sprayers. These will be discussed further in *Heat Transfer* on page 32.

Fume Formation

Previous CFD Modeling

Els et al. (2013) used CFD modelling to simulate fumes rising from the casting beds. Initially they only modelled the heat transfer from the metal and structural surfaces due to convection and radiation. They found that the amount of transferred heat was significantly lower than the energy measured on-site as discussed in the next paragraph. They adjusted the model to include additional heat transfer. Figure 6 (Els et al. 2013) illustrates the results from the verification model and Figure 6 depicts the velocity plot of the fumes from the outside of the shed that covers the entire casting bed area.

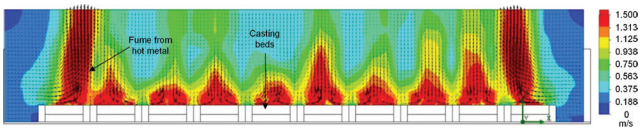

***Figure 6**: Verification model velocity plot (Els et al. 2013)*

Previous Flowtests

Table 2 provides the data that Els et al. (2013) found from on-site measurements. They showed from the comparison of theoretical calculated values and the measured data that the energy released as a results of the formation of the Mn_3O_4 fumes produced about 20% of the total fume energy. Some additional fume energy may be attributed to radiation effects which may play an important role in the fumes' energy content.

***Table 2**: Previous test results (Els et al. 2013)*

Test Point	MOR fan	LCFeMn pour point	Units
Velocity	36.5	32.6	m/s
Temperature	20.1	35.8	$°C$
Static pressure	-3.57	-2.57	kPa
Volume flow	48.5 156861	43.3 134513	Am^3/s Nm^3/h
Mass flow	58.1	49.3	kg/s
Energy	-	2.5	MW

Previous Conclusions

By using the model described above, Els et al. (2013) proved that a 100% fume removal efficiency will require either the extraction volume to be doubled or that the beds should be entirely enclosed. This would have been expensive and the spray system mechanisms (as explained in the following sections) were therefore developed. The spray system's role in visible fume reduction was investigated for the purpose of using this knowledge in future spray model designs. This investigation included air flow patterns, heat transfer and mass transfer of the particulates to the water droplets from the spray.

Air Flow Over the Casting Beds

Water disperses up to 8m outwards from the shed, and as a CFD input, this was broken down into 1m sections with temperature decreasing linearly over the 8m distance. The CFD is simulated with a length along the roof edge of 3m, exposing a $3m^2$ surface area for air flow from under the roof edge into the first control volume as seen in Figure 7.

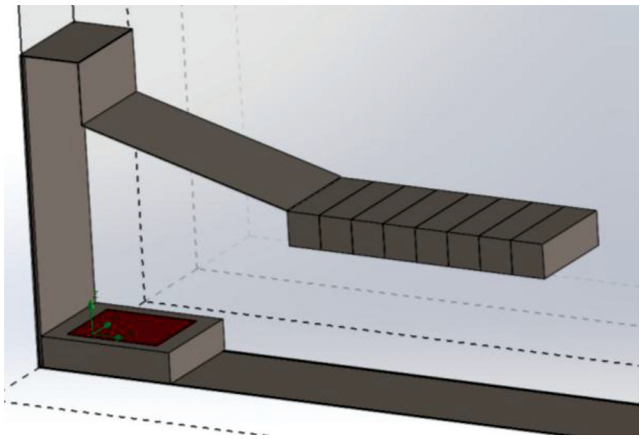

***Figure 7**: 3D representation of the model*

The heat sink was assumed to occur in this control volume. Since the heat sink will have an influence on the circulation pattern (i.e. the flow rate outward from under the roof edge and hence the outward velocity of the air), a trial and error approach

was applied to find the air flowrate into the heat sink. Firstly, the heat sink values for a number of assumed air flow rates were determined using the energy balance described in *Heat Transfer Effects* on page 28. These heat sink values were used as input parameters for the CFD simulations and a velocity profile was determined. By comparing the assumed air flow rates to the resulting CFD output, the approximate velocity of the air could be determined. The calculated heat sink values based on different air inlet flowrates are displayed in Table 3.

***Table 3**: Heat sink results from the energy balance over the control volume*

Description	Values			Units
Air flow rate	3.00	4.00	5.00	(m^3/s)
Air velocity	1.00	1.33	1.67	(m/s)
Block 1	8.90	11.7	14.5	(kW)
Block 2	7.99	10.5	13.0	(kW)
Block 3	7.05	9.25	11.5	(kW)
Block 4	6.10	7.99	9.87	(kW)
Block 5	5.12	6.70	8.27	(kW)
Block 6	4.12	5.38	6.64	(kW)
Block 7	3.10	4.04	4.97	(kW)
Block 8	2.06	2.66	3.26	(kW)

The CFD simulations using the heat sinks in Table 3 are shown in Figure 12, Appendix A. Comparing the CFD results and the calculations explained in Table 3, the air flow rate outwards from under the shed roof was determined to be roughly 4m^3/s for the 3m length of roof modelled.

Heat Transfer

Overview

The heat transfer was modelled in two stages: the first involved using a control volume approach for the first (top) section shown in Figure 5, whilst the second involved using an incremental time approach for the rest of the sections in Figure 5.

First Section

Using the air flow rate as determined in *Air Flow Over the Casting Beds* on page 31, the amount of water that evaporated was calculated and the results appear in Table 4.

***Table 4**: Results after top meter heat transfer*

Description	Value	Units
Hot air temperature	45	$°C$
Relative humidity at hot air temperature	24.4	%
Ambient temperature of air	20	$°C$
Water temperature	12	$°C$
Total heat sink	58.2	kW
Total water mass in	0.375	kg
Total mass evaporated	0.020357	kg
Mass of water out	0.0204	kg
Initial droplet diameter	250	μm
Droplet diameter leaving control volume	245	μm
Average temperature out (T_f)	19.73	$°C$

Lower Section

The air temperature varies slightly from the second meter to the floor, with the air mainly at a temperature of around 20°C and the water temperature at 19.73°C. At 20°C the air is approximately 70% humid and the total driving force for heat transfer is small. This implies that the air will not necessarily reach saturation and the control volume approach would be inaccurate, therefore an incremental time approach would be preferred.

Using *Equation* (12) at incremental steps of 0.01s, the droplet depletion rate is calculated for the remaining 5m (lower) section. This gives the droplet size as well as the mass of water that evaporated after each meter that the droplet falls vertically. The results are displayed in Table 5. From the change in the droplet diameter per meter shown in Table 5, one realises that the change in droplet diameter can be regarded as negligible. Therefore a constant diameter of 245.33µm was used for the mass transfer calculations in the control volumes below the first (upper) one.

Using the approach described above, it was shown (see Appendix A) that the inward air velocity under the edge of the roof increased somewhat with the introduction of the sprays, and that the air flowing over the casting beds will originate from the area where the moisture content is being increased by the water sprays.

***Table 5**: Results for the lower section*

Sections	Mass evaporated (kg)	New drop diameter (μm)
2nd meter	8.0973E-06	245.327
3rd meter	8.2443E-06	245.324
4th meter	8.2441E-06	245.321
5th meter	8.2439E-06	245.319
6th meter	8.2437E-06	245.316

Transfer of Particles to Droplets

The capture efficiency was calculated by considering the relationship in Figure 4 between the capture efficiency and the separation number. *Equation* (16) was used to determine the separation number. The capture efficiency was calculated to be zero. This calculation is validated by de Nevers (2010, 302), who states that for particles less than 1µm the efficiency tends to be zero.

Calculations were done to determine the efficiency of droplet sizes equal to 250µm for different particle sizes given that the inlet flow rate of 15L.min^{-1} was used. The graph in Figure 8 (in effect Figure 4 on an extended scale) shows that for particles

between 0.9µm and 3µm, which are easily inhaled, the capture is negligible.

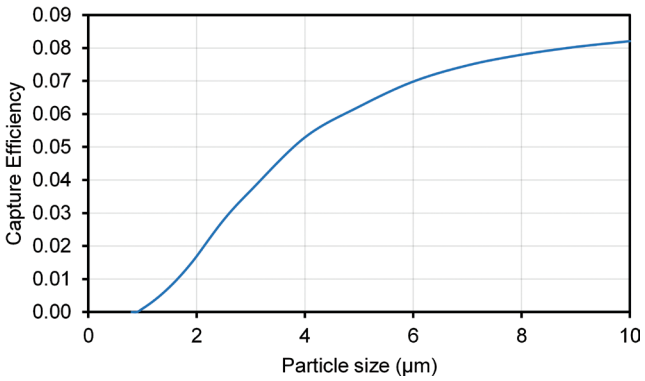

***Figure 8**: Capture efficiency for small particles*

Since the PSD (Figure 3) shows a large number of very fine particles, an investigation was done on smaller droplet sizes and their capture efficiency. The graph in Figure 9 shows the capture efficiency of the small particle sizes at different droplet sizes.

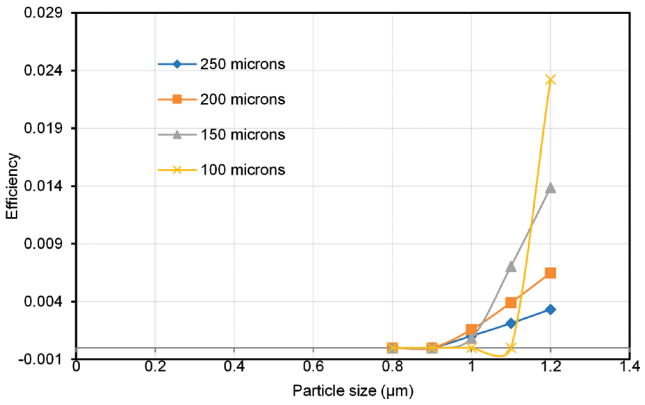

***Figure 9**: Captured efficiency variation with droplet size*

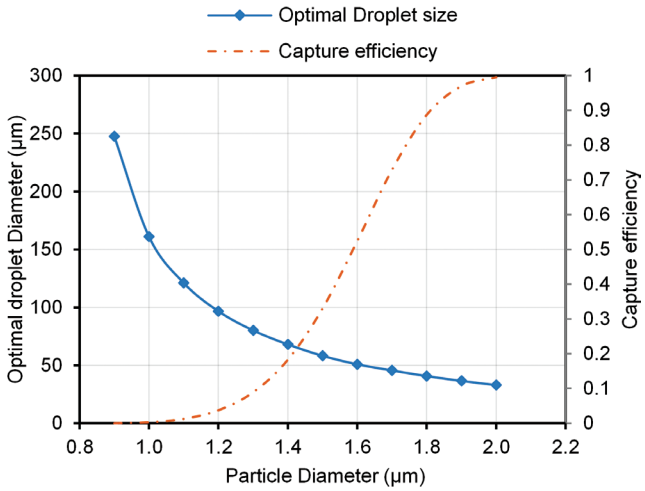

***Figure 10**: Capture efficiency for optimal droplet diameter*

For particles less than 0.8µm, no droplet size showed any capture efficiency. Droplet sizes of 200µm and 250µm captured a small quantity of particles between 0.9µm and 1µm. This is verified by de Nevers (2010, 292), who also suggests that small particles have a tendency to follow a stream line around the object, thereby not easily captured by small droplets.

The calculation procedure was repeated in an attempt to find an optimum droplet size for capture of the critical particle size. The optimal diameter that would result in the largest capture efficiency is shown in Figure 10.

Conclusions

To fully understand the fine water spray system's role in suppressing secondary emission fumes, it is necessary to understand the mechanism involved in the formation of these fumes, as well as possible energy contributors to the fumes' energy content. Considering this, a previous investigation was reflected upon, which involved a combination of heat transfer relationships and CFD modelling to determine possible energy contributors as well as possibilities for better extraction. It was shown that the oxidation reaction involved during the fumes' formation contributed only 20% of the fumes' energy. Based on these plume energy determinations it was found that a 100% fume removal efficiency from the casting shed was possible if either the extraction volume was increased or if the shed was completely enclosed. Unfortunately these solutions are expensive.

A fine water spray system was considered as an alternative solution. After the installation of the spray system a reduction in the amount of visible fume was noticed. Before the installation of the spray system, a slight circulation pattern was observed, which was further enhanced by the spray system. This phenomenon was investigated by considering the heat transfer between the water and the fume-containing air escaping from under the roof. The investigation showed that the heat transfer is most significant near the shed roof and that the main effect was a slight increase in the inward velocity of the air flowing over the casting bed.

Another possible reduction mechanism that was investigated was the transfer of particulates to the water droplets. However, it was found that the capture efficiency tends to zero as a result of the small Mn_3O_4 particulates. Droplet sizes that are about 200µm are able to capture 1µm particles better than smaller droplets, however still at a very low efficiency. Particles that are smaller than 0.8µm will most likely remain suspended in the air.

It is believed that a spray system will work very well for particles larger than 1.4µm. Operations that have fumes containing particles of this magnitude will be able to use a sprayer system as an effective and cheap fume suppressing technique. For operations that contain a large majority of particles between 1µm and 1.5µm, it is recommended that two separate sprayers should be used. The one sprayer should disperse droplets between 200µm and 300µm, while the second sprayer should disperse smaller droplets.

A fine mist sprayer was installed directly over the casting beds

as shown in Figure 11 ensuring a more intense dispersion of moisture. It is clear that the fume concentration is dramatically decreased over the spray area. This leads the authors to believe that the increase in moisture content of the air over the beds – such as when a sprayer system is used – is instrumental in the formation of an oxide layer on the liquid metal, reducing metal vaporisation and thus fume formation. To optimise the sprayer system, further work is necessary to determine the mechanism of fume formation as well as the role of the water spray system to reduce the visible fume emissions.

***Figure 11**: Fine mist sprayers installed at bed top surface level*

References

Çengel Y.A., Ghajar A.J. & Ma H. 2011. Heat and Mass Transfer: *Fundamentals & Applications*, 4th ed., McGraw-Hill.

de Nevers N. 2010. *Air pollution control engineering*. Waveland Press.

Dennis J.H., Hewitt P.J., Redding C.A. & Workman A.D. 2001. A model for prediction of fume formation rate in gas metal arc welding (GMAW), globular and spray modes, DC electrode positive. *Annals of Occupational Hygiene*, 45, 105-113.

Dushman S., Lafferty J.M. & Brown S.C. 1962. Scientific foundations of vacuum technique. *American Journal of Physics*, 30, 612-612.

Els L., Coetzee C. & Vorster O. 'Design of tapping fume extraction systems for ferroalloy furnaces', *Twelfth International Ferroalloy Congress, Helsinki, Finland*, 2010. 6-9.

Els L., Cowx P., Kadkhodabeigi M., Kornelius G., Andrew N., Smith P. & Rencken S. 'Analysis of a ferromanganese secondary fume extraction system to improve design methodologies', *Thirteenth International Ferroalloy Congress, Almaty, Kazakhstan*, 2013. 9-13.

Els L., Cowx P., Smith P. & Nordhagen R. 2014. Analysis and optimization of fume extraction from a ferromanganese furnace tapping operation.
Goering C., Bode L. & Gebhardt M. 1972. Mathematical modeling of spray droplet deceleration and evaporation.

Gonser M. & Hogan T. 2011. *Arc welding health effects, fume formation mechanisms, and characterization methods*. INTECH Open Access Publisher.

Goodfellow H.D. & Tähti E. 2001. *Industrial ventilation design guidebook*. Academic press.

Grant G., Brenton J. & Drysdale D. 2000. Fire suppression by water sprays. *Progress in energy and combustion science*, 26, 79-130.

Green D. & Perry R. 2007. *Perry's Chemical Engineers' Handbook, Eighth Edition*. McGraw-Hill Education.

Guézennec A.-G., Huber J.-C., Patisson F., Sessiecq P., Birat J.-P. & Ablitzer D. 2004. Dust formation by bubble-burst phenomenon at the surface of a liquid steel bath. *ISIJ international*, 44, 1328-1333.

Holterman H. 2003. *Kinetics and evaporation of water drops in air*. IMAG Wageningen.

Huber J., Rocabois P., Faral M., Birat J., Patisson F. & Ablitzer D. 'The formation of EAF dust', *58th Electric Furnace Conference and 17th Process Technology Conference*, 2000. 171-181.

Kopita R. 1955. The Use of an Impingement Baffle Scrubber in Gas Cleaning and Absorption. *Air Repair*, 4, 219-232.

Lee Y.E. & Kolbeinsen L. 2005. Kinetics of oxygen refining process for ferromanganese alloys. *ISIJ international*, 45, 1282-1290.

Mentor Graphics 2015. FloEFD FE 14.1.0.

Modest M.F. 2003. *Radiative Heat Transfer, 2nd Edition*, 2nd ed. Burlington, Academic Press.

Nuyttens D., Baetens K., De Schampheleire M. & Sonck B. 2007. Effect of nozzle type, size and pressure on spray droplet characteristics. *Biosystems Engineering*, 97, 333-345.

Ranz W. & Marshall W. 1952. Evaporation from drops. *Chem. Eng. Prog*, 48, 141-146.

Turkdogan E., Grieveson P. & Darken L. 1963. Enhancement of diffusion-limited rates of vaporization of metals. *The Journal of Physical Chemistry*, 67, 1647-1654.

Welty J.R., Wicks C.E., Rorrer G. & Wilson R.E. 2009. *Fundamentals of momentum, heat, and mass transfer*. John Wiley & Sons.

Williamson R.E. & Threadgill E. 1974. simulation for dynamics of evaporating spray droplets in a gricultural spraying. *Trans ASAE Gen Ed Am Soc Agric Eng*.

Witt P., Solnordal C., Mittoni L., Finn S. & Pluta J. 2006. Optimising the design of fume extraction hoods using a combination of engineering and CFD modelling. *Applied mathematical modelling*, 30, 1167-1179.

Appendix A

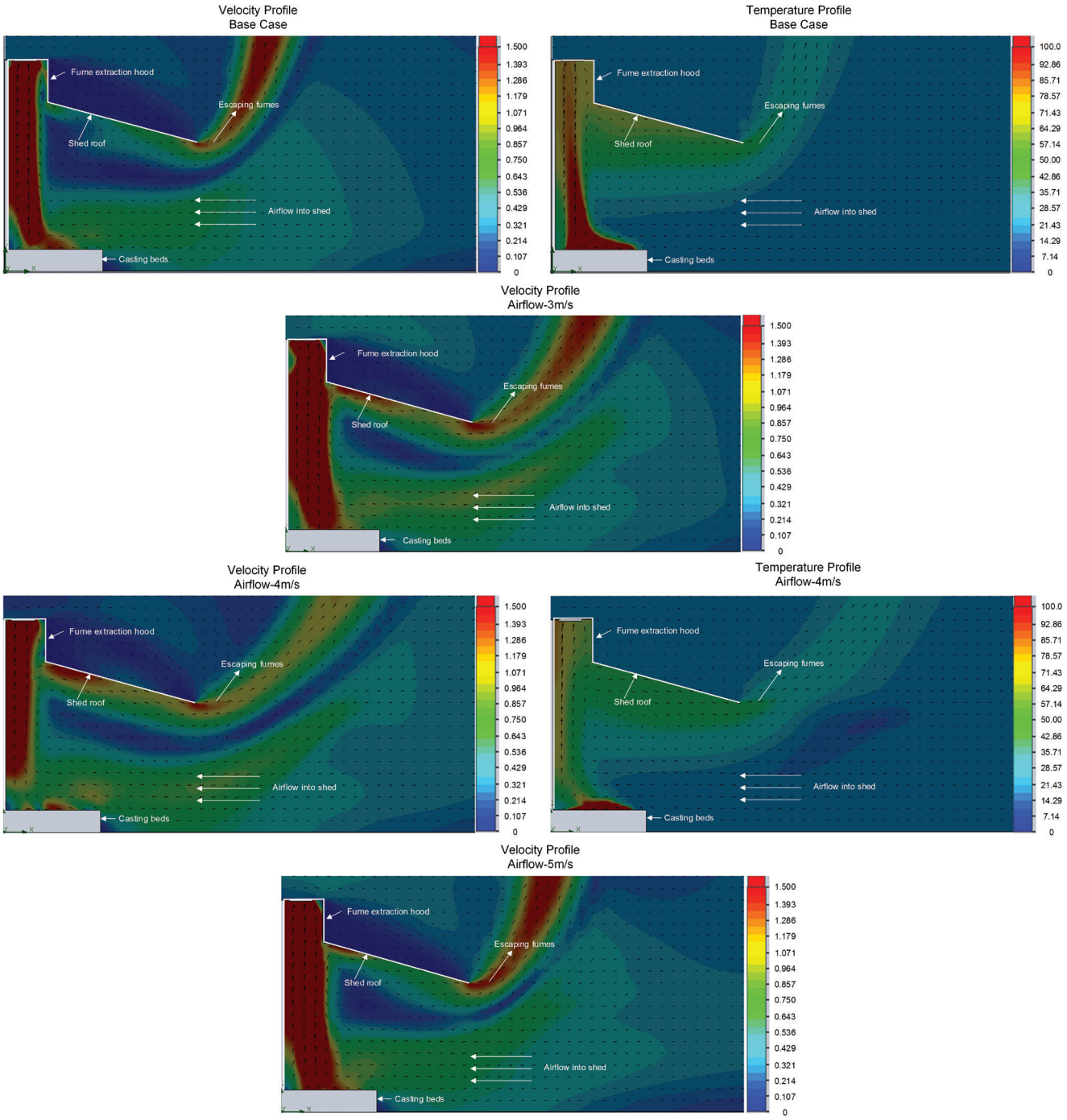

***Figure 12**: CFD results showing the airflow in the casting shed*